
Self-Convolution: A Highly-Efficient Operator for Non-Local Image Restoration

Lanqing Guo¹, Saiprasad Ravishankar² and Bihan Wen^{1*}

¹School of Electrical & Electronic Engineering, Nanyang Technological University, Singapore

²Departments of Computational Mathematics, Science and Engineering,

and Biomedical Engineering, Michigan State University, East Lansing, MI, USA

lanqing001@e.ntu.edu.sg

ravisha3@msu.edu

bihan.wen@ntu.edu.sg

Abstract

Constructing effective image priors is critical to solving ill-posed inverse problems, such as image reconstruction. Recent works proposed to exploit image non-local similarity for inverse problems by grouping similar patches, and demonstrated state-of-the-art results in many applications. However, comparing to classic local methods based on filtering or sparsity, most of the non-local algorithms are time-consuming, mainly due to the highly inefficient and redundant block matching step, where the distance between each pair of overlapping patches needs to be computed. In this work, we propose a novel self-convolution operator to exploit image non-local similarity in a self-supervised way. The proposed self-convolution can generalize the commonly-used block matching step, and produce the equivalent results with much cheaper computation. Furthermore, by applying self-convolution, we propose an effective multi-modality image restoration scheme, which is much more efficient than conventional block matching for non-local modeling. Experimental results demonstrate that (1) self-convolution can significantly speed up most of the popular non-local image restoration algorithms, with two-fold to nine-fold faster block matching; and (2) the proposed multi-modality restoration scheme achieves state-of-the-art denoising results on the RGB-NIR and Stereo image datasets. The code will be released on GitHub.

1 Introduction

Image restoration (IR) aims to recover the underlying clean image $\mathbf{x} \in \mathbb{R}^N$ from its degraded / noisy measurement $\mathbf{y} \in \mathbb{R}^M$, which under a linear imaging model satisfies $\mathbf{y} = \mathbf{A}\mathbf{x} + \mathbf{e}$. Here \mathbf{A} and \mathbf{e} denote the sensing operator and additive noise, respectively. Different forms of \mathbf{A} and \mathbf{e} correspond to a range of important inverse problems, including image denoising, inpainting, super-resolution, compressed sensing, etc. As most of IR problems are ill-posed, exploiting effective image priors as the regularizer is critical to the success of many IR schemes.

Classical IR algorithms take advantage of local image properties. One popular model is *sparsity*, *i.e.*, patches of natural images are known to be sparse in some transform or dictionary domains [9, 21, 18, 34], thus one can reduce noise or artifacts by exploiting the low-dimensionality of the image patches compared to the noise. Beyond local properties, images contain non-local structures, *e.g.*, non-local self-similarity (NSS) in the spatial domain. Many recent IR algorithms [5, 10, 31, 41, 8, 7, 36, 38] exploit NSS by grouping similar patches using block matching (BM), followed by applying a denoiser (*e.g.*, based on low-rankness, joint sparsity, etc.) to each group, which have led to state-of-the-art IR results. However, the BM operator used by the non-local algorithms requires computing the

*Bihan Wen is the corresponding author.

Euclidean distance between every pair of patches, which is computationally very expensive. Besides, to suppress blocky artifacts, almost all non-local IR algorithms work with overlapping patches in BM, which makes the computation highly redundant. These drawbacks limit the efficiency of non-local IR algorithms, especially when processing large-scale and high-dimensional data (*e.g.*, multi-channel images, volumetric data, video).

In this work, we propose a novel Self-Convolution operator for non-local image modeling. We prove that Self-Convolution generalizes several non-local modeling methods, and can be made exactly equivalent to the BM operation. From our experimental results, Self-Convolution can significantly speed up many popular non-local IR algorithms with two-fold to nine-fold faster BM. With such merits of Self-Convolution, we propose an effective denoising scheme for multi-modality (MM) images, called Online Self-MM. It applies the effective STROLLR model [31, 32] for denoising using an online learning framework that is more scalable than batch learning, and outperforms the popular or state-of-the-art denoising algorithms.

2 Related Work

Block matching based image restoration. The well-known BM3D [5] algorithm first applied BM concept to image processing field. Gu et al. [10] incorporated low-rank matrix approximations using the weighted nuclear norm, where BM is used to construct low-rank matrices. Wen et al. [32] proposed a method to jointly exploit the sparsity and low-rankness of data matrices formed by BM. Besides, BM-based methods can be generalized to video processing. VBM4D [17] extended BM3D with motion estimation to track objects as they move throughout the scene. Dong et al. [6] proposed a multi-frame image denoising algorithm that uses BM to extract similar 3D patches. He et al. [12] proposed a hyperspectral image denoising method by grouping similar cubes via BM, and imposing spatial similarity and spectral low-rank structural priors on these groups.

Fast Fourier Transform- (FFT-) accelerated convolution. The well-known and widely-used FFT, proposed by Cooley and Tukey [3], has made a high impact in the signal processing field. Much work in deep learning has been devoted to enhancing the efficiency of and accelerate convolutional layers. Mathieu et al. [19] explored the possibility of using FFTs to reduce the arithmetic complexity of convolutions, which was followed by the work of Vasilache et al. [24].

Self-attention mechanism and non-local network. The self-attention mechanism originally proposed by Vaswani et al. [25] exploits dependencies at each position based on the global context, and is widely used in several image applications [39, 20]. The non-local network was first proposed by Wang et al. [27] for video and image tasks, followed by a number of extensions [16]. While both self-attention mechanism and non-local networks exploit feature-domain non-local correlation, the proposed Self-Convolution focuses on the spatial self-similarity of natural images.

3 Self-Convolution

We start by reviewing several non-local methods based on existing works, and then propose a non-local modeling framework to unify these methods using Self-Convolution that leads to highly-efficient computation. To facilitate the discussion, we define the vectorization operation on matrices and tensors (unfolding along the first mode), as $\text{vec}(\cdot) : \mathbb{R}^{\sqrt{n} \times \sqrt{n}} \rightarrow \mathbb{R}^n$ and $\text{vecT}(\cdot) : \mathbb{R}^{\sqrt{n} \times \sqrt{n} \times p} \rightarrow \mathbb{R}^{np}$, respectively. The bold uppercase letters (*e.g.*, \mathbf{X}) denote matrices, while the bold lowercase letters (*e.g.*, \mathbf{x}) denote vectors. We use (j, k) to denote the 2D indices or locations in a matrix, and similarly, (j) to denote the 1D indices of a vector.

3.1 Preliminary

Non-local image modeling has demonstrated promising performance for IR tasks by exploiting NSS properties. Classic non-local methods, *e.g.*, the well-known non-local means (NLM) algorithm [2], exploit the correlation among neighbouring patches with adaptive weighting. For each reference patch $\mathbf{X}_i \in \mathbb{R}^{\sqrt{n} \times \sqrt{n}}$ from an image $\mathbf{X} \in \mathbb{R}^{\sqrt{N} \times \sqrt{N}}$, NLM computes the weighting coefficients with respect to other patches as follows

$$\mathbf{s}_i(j) = \Theta_i^{-1} \exp(-\|\mathbf{X}_j - \mathbf{X}_i\|_F^2 / b^2), \quad \Theta_i = \sum_j \exp(-\|\mathbf{X}_j - \mathbf{X}_i\|_F^2 / b^2) \quad \forall i, \quad (1)$$

where b is a hyper-parameter scaling the distance metric. Such approach recovers each \mathbf{X}_i using the weighted average of non-local patches as $\sum_j s_i(j)\mathbf{X}_j$.

More recent non-local works apply block matching (BM), which only selects the K ($K \ll N$) most similar patches to \mathbf{X}_i , with the indices of the similar patches stored in the set $\hat{\mathcal{S}}_i$, $|\hat{\mathcal{S}}_i| \leq K$. BM is computed by solving

$$\hat{\mathcal{S}}_i^E = \arg \min_{\mathcal{S}_i: |\mathcal{S}_i| \leq K} \sum_{j \in \mathcal{S}_i} d_E(\mathbf{X}_j, \mathbf{X}_i) = \arg \min_{\mathcal{S}_i: |\mathcal{S}_i| \leq K} \sum_{j \in \mathcal{S}_i} \|\mathbf{X}_j - \mathbf{X}_i\|_F^2 \quad \forall i \quad (2)$$

Here the Euclidean distance serves as the similarity metric. Other functions have also been used in different algorithms, *e.g.*, transform-domain distance [5], or the normalized cross correlation [29]. The latter for the case of (non-negative) natural images leads to

$$\hat{\mathcal{S}}_i^{NCC} = \arg \min_{\mathcal{S}_i: |\mathcal{S}_i| \leq K} \sum_{j \in \mathcal{S}_i} d_{NCC}(\mathbf{X}_j, \mathbf{X}_i) = \arg \min_{\mathcal{S}_i: |\mathcal{S}_i| \leq K} - \sum_{j \in \mathcal{S}_i} \frac{\text{vec}(\mathbf{X}_j)^T \text{vec}(\mathbf{X}_i)}{\|\mathbf{X}_j\|_F \|\mathbf{X}_i\|_F} \quad \forall i. \quad (3)$$

For BM-based non-local methods, a denoiser (*e.g.*, based on low-rank or sparse modeling) is applied to each patch group $\{\mathbf{X}_j\}_{j \in \hat{\mathcal{S}}_i}$ to exploit the group-wise similarity for image recovery.

3.2 A Unified Non-Local Modeling via Self-Convolution

Though there are various approaches to exploit image non-local self-similarity, the core of these methods is to compute the distance or similarity between each patch pair using different metrics or losses. We propose a novel (2D) **Self-Convolution** operator which efficiently computes the similarity between each \mathbf{X}_i and the image as $\mathbf{C}_i \triangleq \mathbf{X} * \mathbf{X}_i \in \mathbb{R}^{\sqrt{M} \times \sqrt{M}}$, where $\sqrt{M} \triangleq (\sqrt{N} - \sqrt{n} + 1)$, which can be computed as follows²

$$\mathbf{C}_i(j, k) = \sum_{l=1}^{\sqrt{n}} \sum_{m=1}^{\sqrt{n}} \mathbf{X}_i(l, m) \mathbf{X}(j+l-1, k+m-1). \quad (4)$$

Based on the Self-Convolution, we propose a general optimization problem to unify the commonly used non-local modeling methods as follows³

$$\hat{\mathbf{a}}_i = \arg \min_{\mathbf{a}_i} \|H(\mathbf{C}_i, \mathbf{X}, \mathbf{X}_i) - \mathbf{a}_i\|_F^2 + \rho(\mathbf{a}_i) \quad \forall i. \quad (5)$$

Here, the penalty $\rho(\mathbf{a}_i)$ denotes a regularizer for \mathbf{a}_i , and $H(\mathbf{C}_i, \mathbf{X}, \mathbf{X}_i) \in \mathbb{R}^M$ denotes the distance / similarity measuring function based on Self-Convolution that also vectorizes the similarity map. Both $\rho(\mathbf{a}_i)$ and $H(\mathbf{C}_i, \mathbf{X}, \mathbf{X}_i)$ vary for different non-local modeling approaches.

Next, we prove that the proposed Self-Convolution formulation (5) can be made equivalent to various commonly used non-local image operations. To facilitate the analysis, we define a normalization vector $\mathbf{h}_{X_i} = \|\mathbf{X}_i\|_F \mathbf{h}_X$ for each \mathbf{X}_i , where $\mathbf{h}_X \in \mathbb{R}^M$ is defined as $\mathbf{h}_X(j) \triangleq \|\mathbf{X}_j\|_F$. We let \odot denote the element-wise product of two vectors or matrices. For the following results, we provide the proof sketch, while the corresponding **full proofs** are all included in the **Appendix**.

Lemma 1. *The normalized cross-correlation in (3) is $d_{NCC}(\mathbf{X}_j, \mathbf{X}_i) = -[\text{vec}(\mathbf{C}_i) \odot \mathbf{g}_{X_i}](j)$, where $\mathbf{g}_{X_i}(j) = 1/\mathbf{h}_{X_i}(j) \forall j$.*

Proof Sketch. As the ‘‘convolution’’ operation used in neural network is equivalent to the ‘‘correlation’’ operation in signal processing, the proposed Self-Convolution metric becomes equivalent to the non-local cross correlation metric, subject to patch-wise normalization using \mathbf{h}_{X_i} . \square

Lemma 2. *The Euclidean distance in (2) is $d_E(\mathbf{X}_j, \mathbf{X}_i) = [\mathbf{h}_X \odot \mathbf{h}_X + \|\mathbf{X}_i\|_F^2 \mathbf{1} - 2\text{vec}(\mathbf{C}_i)](j) \forall j$.*

Proof Sketch. The Euclidean distance is related to cross correlation as $\|\mathbf{X}_j - \mathbf{X}_i\|_F^2 = \|\mathbf{X}_j\|_F^2 + \|\mathbf{X}_i\|_F^2 - 2\text{vec}(\mathbf{X}_j)^T \text{vec}(\mathbf{X}_i)$. Based on the result of Lemma 1, it is easy to convert Self-Convolution to Euclidean distance by adding the normalization terms. \square

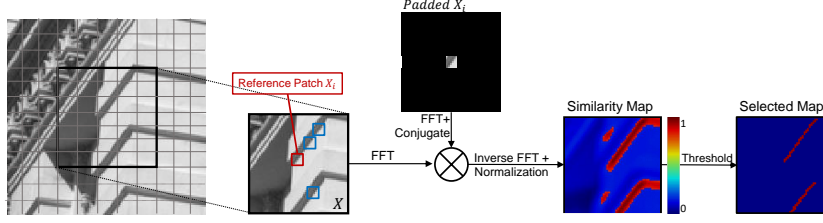


Figure 1: Illustration of the proposed Self-Convolution scheme using FFTs.

Proposition 1. *Self-Convolution formulation in (5) is equivalent to the weight calculation in NLM (1) if $\rho(\mathbf{a}_i) = 0$ and $H(\mathbf{C}_i, \mathbf{X}, \mathbf{X}_i) = \frac{1}{\sigma_i} \exp\{(\text{vec}(\mathbf{C}_i) - \mathbf{h}_X \odot \mathbf{h}_X - \|\mathbf{X}_i\|_F^2 \mathbf{1})/b^2\}$. Thus, the result of (5) becomes the NLM weighting, i.e., $\hat{\mathbf{a}}_i = \hat{\mathbf{s}}_i$ coincides with (1).*

Proof Sketch. NLM makes use of all non-local patches, thus $\rho(\mathbf{a}_i) = 0$. Based on Lemmas 2 and (1), the weights of NLM can be computed using $H(\mathbf{C}_i, \mathbf{X}, \mathbf{X}_i)$ by Self-Convolution. \square

Theorem 1. *Self-Convolution formulation is equivalent to block matching when*

1. $\rho(\mathbf{a}_i) = \Phi_K(\mathbf{a}_i)$, where $\Phi_K = 0$ if $\|\mathbf{a}_i\|_0 \leq K$ and $\Phi_K = +\infty$ otherwise.
2. $H(\mathbf{C}_i, \mathbf{X}, \mathbf{X}_i) = \text{vec}(\mathbf{C}_i) - \frac{1}{2} \mathbf{h}_X \odot \mathbf{h}_X$ using Euclidean distance; Or
3. $H(\mathbf{C}_i, \mathbf{X}, \mathbf{X}_i) = \text{vec}(\mathbf{C}_i) \odot \mathbf{g}_{X_i}$ using normalized cross correlation.

Thus, the support of the solution to (5), i.e., $\text{supp}(\hat{\mathbf{a}}_i)$ is the solution \hat{S}_i^E in (2) or \hat{S}_i^{NCC} in (3).

Proof Sketch. The penalty term $\Phi_K(\mathbf{a}_i)$ is a barrier function, equivalent to imposing an ℓ_0 sparsity constraint, i.e., $\|\mathbf{a}_i\|_0 \leq K$. Sparse coding keeps the K largest elements in $H(\mathbf{C}_i, \mathbf{X}, \mathbf{X}_i)$ by projection onto the ℓ_0 unit ball, which is equivalent to selecting the K most similar patches. Therefore, the locations of the non-zero elements in $\hat{\mathbf{a}}_i$ correspond to the BM set in (2) or (3). \square

Lemmas 1 and 2 show the relationship of Self-Convolution metric H to various BM metrics. Proposition 1 and Theorem 1 show the equivalence of Self-Convolution formulation (5) to NLM and BM, and how (5) generalizes the popular non-local image modeling schemes using Self-Convolution.

3.3 Efficient Self-Convolution via FFT

Directly computing Self-Convolution in the spatial domain using (4) is as expensive as the conventional BM or NLM operations. Instead, we propose to apply the Fast Fourier Transform (FFT) to accelerate Self-Convolution operations. Let $\mathbf{F} \in \mathbb{C}^{N \times N}$ and \mathbf{F}^H denote the 2D Fourier matrix and the inverse FFT (IFFT) matrix, respectively, and $\mathbf{x} = \text{vec}(\mathbf{X}) \in \mathbb{R}^N$. Besides, we use $P(\cdot) : \mathbb{R}^{\sqrt{n} \times \sqrt{n}} \mapsto \mathbb{R}^{\sqrt{N} \times \sqrt{N}}$ to denote a zero-padding operator, i.e., it pads zeros to the surrounding of a small patch to match the image size. We denote $\mathbf{x}_i = \text{vec}(P(\mathbf{X}_i)) \in \mathbb{R}^N$ as the vectorized image patch after padding, and $\bar{\mathbf{u}}$ denotes the complex conjugate of vector \mathbf{u} .

Proposition 2. *Self-Convolution using (4) is equivalent to the following FFT-based operations (we use \bar{u} to denote the complex conjugate of u):*

$$\mathbf{C}_i = \mathbf{F}^H (\mathbf{F} \mathbf{x} \odot \overline{\mathbf{F} \mathbf{x}_i}). \quad (6)$$

Proof Sketch. The equivalence is obvious using the classic convolution theorem [15]. \square

Comparing to (4), the FFT-based Self-Convolution (6) only computes an image-level element-wise product once, which is more efficient. Furthermore, as an additional advantage to the computation in (4), we pre-compute $\mathbf{F} \mathbf{x}$ as it is fixed for calculating different \mathbf{C}_i corresponding to different

²We follow the definition of ‘‘convolution’’ in neural networks, i.e., the ‘‘correlation’’ in signal processing.

³Self-Convolution is applied to the entire \mathbf{X} in (5), for simplicity of analysis. Some non-local algorithms only apply BM within a neighbourhood search window Ω_i for each \mathbf{X}_i . The proposed Self-Convolution can be generalized to such setup using $\mathbf{X}_{\Omega_i} * \mathbf{X}_i$, where \mathbf{X}_{Ω_i} denotes the sub-image containing all patches within Ω_i .

Operation Type	Computational Cost
Block Matching	$\mathcal{O}(nN^2)$
Self-Convolution (4)	$\mathcal{O}(nN^2)$
Self-Convolution (FFT)	$\mathcal{O}\{N\log N + (n\log N + N + N\log N)N\}$

Table 1: Computational costs for various methods (over all reference patches). Here, n and N denote the number of pixels in a patch and the number of patches within the image.

reference patches X_i within the same image. Fig. 1 shows an example of the FFT-based Self-Convolution: the magnitudes of \mathbf{C}_i after normalization (Theorem1) reflect the similarity between \mathbf{X}_i and all non-local patches. Based on Proposition 2, the non-local modeling framework, which is equivalent to (5), using the FFT-based Self-Convolution can be formulated as

$$\hat{\mathbf{a}}_i = \arg \min_{\mathbf{a}_i} \left\| H(\mathbf{F}^H(\mathbf{F}\mathbf{x} \odot \overline{\mathbf{F}\mathbf{x}_i}), \mathbf{X}, \mathbf{X}_i) - \mathbf{a}_i \right\|_F^2 + \rho(\mathbf{a}_i) \quad \forall i \quad (7)$$

3.4 Computational Cost Analysis

We assume that the patch stride equals to 1, thus the number of total patches is approximately equal to the image size N . The computational cost of the conventional BM algorithm scales as $\mathcal{O}(nN^2)$, while the direct convolution requires $\mathcal{O}(nN^2)$ operations. The proposed FFT-based Self-Convolution includes the following costs: a one-time FFT for \mathbf{X} that scales as $\mathcal{O}(N\log N)$; N FFTs, one for each of the zero-padded (sparse) image patches (\mathbf{x}_i), which require $\mathcal{O}(nN\log N)$ operations [13]; N pointwise vector products in the frequency domain requiring $\mathcal{O}(N^2)$ multiplies; and N inverse FFTs (one for each \mathbf{x}_i) which require $\mathcal{O}(N^2\log N)$. The overall complexity is thus $\mathcal{O}\{N\log N + (n\log N + N + N\log N)N\}$, which scales as $\mathcal{O}\{(\log N + 1)N^2\}$. Table 1 summarizes the computational complexity comparison of these non-local operations. As typically $\log N + 1 < n$, with the gap especially larger when the algorithm is working with 3D patches, *e.g.*, video or multi-modality data processing, the FFT-based Self-Convolution has much lower computational cost.

4 Self-Convolution for Multi-Modality Image Denoising

We propose a multi-modality image denoising scheme, called Online Self-MM, which has an efficient algorithm using FFT-based Self-Convolution. Fig. 1 shows the algorithm pipeline, which contains three steps, namely (1) Self-Convolution, (2) Online Denoising, and (3) Image Reconstruction.

Self-Convolution: A multi-modality image can be represented as a tensor $\mathcal{X} \in \mathbb{R}^{\sqrt{N} \times \sqrt{N} \times p}$, and the proposed algorithm aims to restore its noisy version \mathcal{Y} . We apply **2D** Self-Convolution to \mathcal{Y} , *i.e.*, 2D convolution along each spatial channel followed by summing the result over channels, working with the overlapping 3D patches $\mathcal{Y}_i \in \mathbb{R}^{\sqrt{n} \times \sqrt{n} \times p}$ which are extracted from \mathcal{Y} . The noisy tensor and padded 3D patch are vectorized as $\mathbf{y} = \text{vecT}(\mathcal{Y})$ and $\mathbf{y}_i = \text{vecT}(P(\mathcal{Y}_i)) \in \mathbb{R}^{Np}$, and the **2D** Self-Convolution is obtained by solving the following problem,

$$\hat{\mathbf{a}}_i = \arg \min_{\mathbf{a}_i} \left\| S(\mathbf{F}^H(\mathbf{F}\mathbf{y} \odot \overline{\mathbf{F}\mathbf{y}_i}) - 0.5 \mathbf{h}_{\mathbf{y}} \odot \mathbf{h}_{\mathbf{y}}) - \mathbf{a}_i \right\|_F^2 \quad s.t. \quad \|\mathbf{a}_i\|_0 \leq K \quad \forall i. \quad (8)$$

where \mathbf{F} denotes 2D (spatial) channel-wise FFT for a 3D input and $S(\cdot)$ performs summation along the channel dimension. Here we impose a sparsity constraint, which is equivalent to applying a barrier function $\rho(\mathbf{a}_i)$ in (7). The solution to (8) is obtained by retaining only the K -largest magnitude elements in $S(\mathbf{F}^H(\mathbf{F}\mathbf{y} \odot \overline{\mathbf{F}\mathbf{y}_i}) - 0.5 \mathbf{h}_{\mathbf{y}} \odot \mathbf{h}_{\mathbf{y}})$, and setting the others to zero [30]. Alternatively, one can also apply **3D** Self-Convolution to \mathcal{Y} , by working with patches $\mathcal{Y}_i \in \mathbb{R}^{\sqrt{n} \times \sqrt{n} \times r}$ where $r < p$. In this case, Self-Convolution allows to search across channels by applying a 3D FFT (and omitting the $S(\cdot)$ function) in (8). We construct the groups of similar patches \mathbf{Y}_i using $\hat{\mathcal{S}}_i = \text{supp}(\hat{\mathbf{a}}_i)$ as

$$\mathbf{Y}_i = [\mathbf{y}_{\hat{\mathcal{S}}_i(1)}, \mathbf{y}_{\hat{\mathcal{S}}_i(2)}, \dots, \mathbf{y}_{\hat{\mathcal{S}}_i(K)}] \quad \forall i. \quad (9)$$

Online Denoising: Recent works [31, 32] proposed an effective non-local image model, called STROLLR, using *transform learning*. However, the batch STROLLR algorithm involves inefficient BM, which limits the algorithm’s scalability to handle high-dimensional or multi-modality images. For large-scale images, we need to process a big amount of \mathbf{Y}_i ’s. Thus, we propose to extend the batch STROLLR to online learning, and apply online STROLLR to process \mathbf{Y}_τ sequentially for

$\tau = 1, 2, \dots, t, \dots, N$. When denoising \mathbf{Y}_t , the online algorithm solves the following problem:

$$\begin{aligned} \{\hat{\mathbf{Z}}_t, \hat{\mathbf{W}}_t, \hat{\alpha}_t, \hat{\mathbf{D}}_t\} = & \arg \min_{\{\mathbf{Z}_t, \mathbf{W}_t, \alpha_t, \mathbf{D}_t\}} \|\mathbf{Y}_t - \mathbf{Z}_t\|_F^2 + \gamma_l \left\{ \|\mathbf{Z}_t - \mathbf{D}_t\|_F^2 + \theta^2 \text{rank}(\mathbf{D}_t) \right\} \\ & + \gamma_s \sum_{\tau=1}^t \left\{ \|\mathbf{W}_t \mathbf{z}_\tau - \alpha_\tau\|_2^2 + \beta^2 \|\alpha_\tau\|_0 \right\} \quad \text{s.t.} \quad \mathbf{W}_t^T \mathbf{W}_t = \mathbf{I}_{np}. \end{aligned} \quad (10)$$

Here \mathbf{Z}_t is the denoised estimate of \mathbf{Y}_t with $\mathbf{z}_\tau = \text{vec}(\mathbf{Z}_\tau)$, and $\gamma_l, \gamma_s, \theta$, and β are hyper-parameters. In (10), \mathbf{D}_t and α_t denote the low-rank approximation and sparse codes for \mathbf{Z}_t , respectively. The transform $\mathbf{W}_t \in \mathbb{R}^{nK \times nK}$ is learned online by adapting to all $\{\mathbf{z}_\tau\}_{\tau=1}^t$. We propose to solve (10) using an efficient block coordinate descent algorithm with initialization for variables based on most recent estimates, which is similar to the batch STROLLR algorithm [32]. First, fixing $\mathbf{Z}_t = \mathbf{Y}_t$, we solve for \mathbf{D}_t in (10) by finding the best low-rank approximation to \mathbf{Z}_t as follows:

$$\hat{\mathbf{D}}_t = \arg \min_{\mathbf{D}_t} \|\mathbf{Z}_t - \mathbf{D}_t\|_F^2 + \theta^2 \text{rank}(\mathbf{D}_t) \quad (11)$$

Let $\mathbf{Z}_t = \mathbf{\Lambda}_t \text{diag}(\mathbf{w}_t) \mathbf{\Delta}_t^T$ be a full singular value decomposition (SVD), where the diagonal vector \mathbf{w}_t contains the singular values. Then the exact solution to (11) is $\hat{\mathbf{D}}_t = \mathbf{\Lambda}_t \text{diag}\{H_\theta(\mathbf{w}_t)\} \mathbf{\Delta}_t^T$, where the $H_\theta(\cdot)$ denotes the hard thresholding operator at threshold θ . With \mathbf{W}_t fixed at $\hat{\mathbf{W}}_{t-1}$ and fixed \mathbf{z}_t , we then solve the following sparse coding problem for $\hat{\alpha}_t$:

$$\hat{\alpha}_t = \arg \min_{\alpha_t} \|\mathbf{W}_t \mathbf{z}_t - \alpha_t\|_2^2 + \beta^2 \|\alpha_t\|_0, \quad (12)$$

which is known as the transform-model sparse coding problem, and the exact solution $\hat{\alpha}_t = H_{\beta^2}(\mathbf{W}_t^T \mathbf{z}_t)$. Next, the transform matrix is updated in (10) by solving the following problem:

$$\hat{\mathbf{W}}_t = \arg \min_{\mathbf{W}_t} \frac{1}{t} \sum_{\tau=1}^t \|\mathbf{W}_t \mathbf{z}_\tau - \hat{\alpha}_\tau\|_2^2 \quad \text{s.t.} \quad \mathbf{W}_t^T \mathbf{W}_t = \mathbf{I}_{np}. \quad (13)$$

Denoting the full SVD of $\mathbf{V}_t \triangleq \sum_{\tau=1}^t \mathbf{z}_\tau \hat{\alpha}_\tau^T$ as $\mathbf{\Phi}_t \mathbf{\Sigma}_t \mathbf{\Psi}_t^T$, the exact solution to (13) is obtained as $\hat{\mathbf{W}}_t = \mathbf{\Psi}_t \mathbf{\Phi}_t^T$ [22]. For transform update step (13), the SVD of the matrix $\mathbf{V}_t = (1 - t^{-1})\mathbf{V}_{t-1} + t^{-1}\mathbf{z}_t \hat{\alpha}_t^T$ can be efficiently updated (without storing all the past estimated variables) via a fast rank-1 update to the SVD of \mathbf{V}_{t-1} [33]. Finally, with the fixed $\hat{\mathbf{D}}_t, \hat{\alpha}_t$, and $\hat{\mathbf{W}}_t$, the denoised patch group $\hat{\mathbf{Z}}_t$ is updated by solving

$$\hat{\mathbf{Z}}_t = \arg \min_{\mathbf{Z}_t} \|\mathbf{Y}_t - \mathbf{Z}_t\|_F^2 + \gamma_l \left\| \mathbf{Z}_t - \hat{\mathbf{D}}_t \right\|_F^2 + \gamma_s \left\| \hat{\mathbf{W}}_t \mathbf{z}_t - \hat{\alpha}_t \right\|_2^2, \quad (14)$$

which has a least-square solution as $\hat{\mathbf{Z}}_t = [\mathbf{Y}_t + \gamma_l \hat{\mathbf{D}}_t + \gamma_s \text{vec}^{-1}(\hat{\mathbf{W}}_t^T \hat{\alpha}_t)] / (1 + \gamma_l + \gamma_s)$.

The proposed online algorithm denoises each \mathbf{Y}_τ sequentially, and update the sparsifying transform every time a new \mathbf{Y}_τ arrives. Alternatively, similar to [33], the strictly online denoising can be modified into a mini-batch algorithm based on (10), which process a set of \mathbf{Y}_τ 's each time, and only updates the transform once per mini-batch. Compared to the strictly online algorithm, the mini-batch learning scheme requires higher memory complexity, but enjoys a lower computational cost.

Image Reconstruction: The online denoising algorithm sequentially outputs each patch group $\hat{\mathbf{Z}}_i = [\hat{\mathbf{Z}}_i(\cdot, 1), \hat{\mathbf{Z}}_i(\cdot, 2), \dots, \hat{\mathbf{Z}}_i(\cdot, K)]$, which is the denoised estimate of the input $\hat{\mathbf{Y}}_i = [\mathbf{y}_{\hat{\mathcal{S}}_i(1)}, \mathbf{y}_{\hat{\mathcal{S}}_i(2)}, \dots, \mathbf{y}_{\hat{\mathcal{S}}_i(K)}]$. Correspondingly, each $\hat{\mathbf{Z}}_i(\cdot, j)$ is the denoised estimate of $\mathbf{y}_{\hat{\mathcal{S}}_i(j)}$, and these denoised patches are aggregated back at their respective locations in the image.

For the Online Self-MM scheme, we first tensorize each $\hat{\mathbf{Z}}_i(\cdot, j)$ as $\hat{\mathcal{Z}}_i(\cdot, j) = \text{vecT}^{-1}(\hat{\mathbf{Z}}_i(\cdot, j)) \in \mathbb{R}^{\sqrt{n} \times \sqrt{n} \times p}$, and then deposit each denoised $\hat{\mathcal{Z}}_i(\cdot, j)$ back to the corresponding location of the image at $\hat{\mathcal{S}}_i(j)$. As we are working with overlapping patches, the pixel values of the aggregated image are normalized by the number of aggregated patches containing each pixel, which then generates the final denoised MM image.

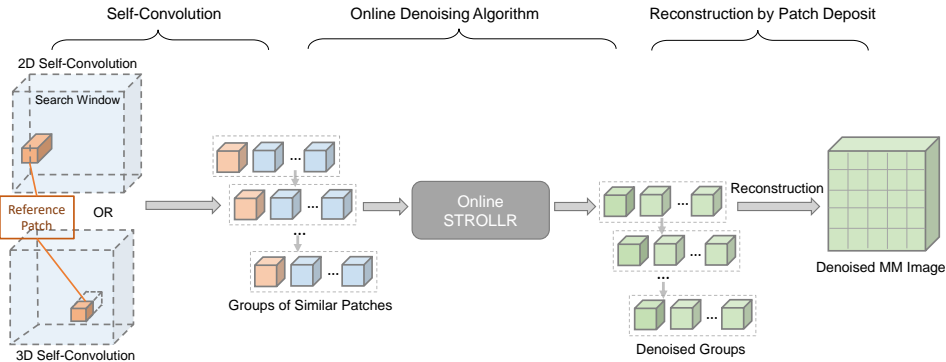


Figure 2: Illustration of the Online Self-MM scheme for multi-modality (MM) image restoration.

5 Experiments

5.1 Speed-Up of Non-Local Algorithms by Self-Convolution

We first demonstrate how the proposed Self-Convolution can significantly speed up non-local IR algorithms in general. We select popular single-channel IR algorithms, including WNNM [10], STOLLR [31], GHP [41], NCSR [8], SAIST [7], PGPD [36] and RRC [38], which all involve 2D BM. Furthermore, we select multi-channel algorithms, including MCWNNM [35] for multi-channel image denoising, SALT [33] for video denoising, as well as our method for multi-modality image denoising, which all involve high-dimensional BM. We work on 512×512 gray images, and $256 \times 256 \times q$ multi-channel data (The data modalities are different, with $q = 3, 20, 4$ for MCWNNM, SALT, and our Self-MM, respectively)⁴, to test the original runtime of recovering by these methods. For a fair comparison, we fixed the patch stride to 1 pixel, search window size as 30×30 , and patch size as 6×6 for all methods⁵. Furthermore, we replace the conventional BM used in these methods with the proposed Self-Convolution, and record the accelerated runtime comparing to the original ones in Table 2. All competing algorithms can generate the exactly the same result using Self-Convolution, which proves the implementation equivalence in practice. Besides, we calculate the runtime portion of BM, using the original implementations, for each algorithm denoted as BMtime%. For most of the non-local algorithms, BM occupies a major portion of the runtime, which limits the overall efficiency. Table 2 lists the original and accelerated BM runtime of the selected algorithms. We show that the proposed Self-Convolution can provide $2\times$ to $9\times$ speedup for BM, especially for multi-channel IR algorithms. All the experiments are carried out in the Matlab (R2019b) environment running on a PC with Intel(R) Core(TM) i9-10920K CPU 3.50GHz.

Method	Original Runtime	Self-Conv Runtime	BMtime%	Original BM	Self-Conv	Speed-Ups
WNNM [10]	63.2	43.8	36.9%	23.3	7.8	3×
STOLLR [31]	87.7	68.9	36.7%	38.2	13.3	3×
GHP [41]	412.6	218.3	69.9%	288.6	94.2	3×
NCSR [8]	134.7	82.4	57.1%	76.9	28.1	3×
SAIST [7]	708.2	562.2	32.0%	227.0	78.6	3×
PGPD [36]	305.2	89.6	85.3%	260.3	41.3	6×
RRC [38]	601.2	505.6	26.9%	161.8	74.2	2×
MCWNNM [35]	2899.0	2371.3	15.8%	458.6	61.6	8×
SALT [33]	375.9	113.8	75.4%	294.8	33.2	9×
Ours	139.0	44.3	78.8%	109.5	16.3	7×

Table 2: Runtime (in seconds) comparisons of non-local algorithms using BM and Self-Convolution, for denoising 512×512 single-channel images and $256 \times 256 \times q$ multi-channel images, where BMtime% denotes the runtime portion of BM.

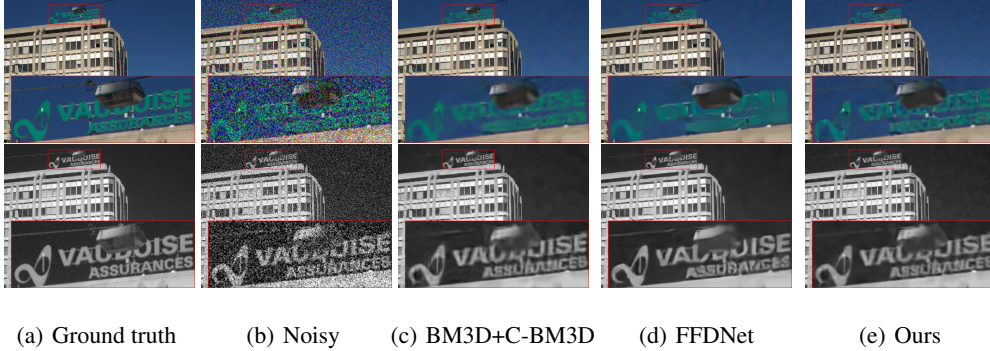


Figure 3: Examples of the RGB-NIR image denoising ($\sigma = 50$) results: top and bottom rows are RGB and NIR channels, respectively, of the (a) ground truth, (b) noisy inputs, and the denoised results using (c) C-BM3D [4], (d) FFDNet [40], and (e) our Online Self-MM.

σ	Classic		Deep Learning		Guided		Online Self-MM			
	BM3D [5]	BM3D+ C-BM3D [5, 4]	FFDNet [40]	FOCNet [14]	Guided Filter [11]	Cross Field [37]	Only RGB	w/o TL	w/o LR	Proposed
5	39.46	40.08	40.07	-	34.01	36.70	40.50	40.39	39.69	40.51
10	35.70	36.54	36.81	-	32.79	33.31	36.89	36.74	36.23	36.89
15	33.68	34.60	34.96	-	31.56	31.67	34.79	34.56	34.24	35.07
20	32.34	33.29	33.69	-	30.39	30.09	33.33	33.01	32.84	33.69
50	28.47	29.48	29.90	29.29	25.24	23.97	29.23	29.27	28.92	29.77

Table 3: PSNRs (in dB) of the RGB-NIR image denoising results, averaged over 18 images selected from the RGB-NIR Scene Dataset [1]. For those noise levels for which FOCNet’s trained models are not publicly available, we put “-” as the corresponding results are unavailable.

5.2 Multi-Modality Image Denoising

We apply the proposed Online Self-MM to denoising multi-modality images from two public-available datasets, *i.e.*, IVRG RGB-NIR Dataset [1] and Flickr1024 Stereo Dataset [28, 26]. Due to space constraints, we present the results and discussion on IVRG RGB-NIR in the main paper, while leaving the results on Flickr1024 Stereo in the **Appendix**. We randomly select 18 pairs of the near-infrared (NIR) and RGB images, containing all 9 image categories, from the IVRG RGB-NIR Dataset [1] for testing. All selected images are around $1024 \times 768 \times 4$, and we simulate i.i.d. additive Gaussian noise for all channels, using various noise levels $\sigma = 5, 10, 15, 20$, and 50 , to generate noisy measurements for each image. We work with $6 \times 6 \times 4$ 3D patches and apply 2D Self-Convolution with a 30×30 search window to select the groups of similar patches. We follow the guideline in [32], and set the hyper-parameters in Online Self-MM to be $\gamma_s = \gamma_l = 1$. Similar to [32], for low-level noise, *i.e.*, $0 \leq \sigma \leq 20$, we apply one-pass denoising scheme with $\beta = 3.3$ and $\theta = 1.5\sigma$; for high-level noise, *i.e.*, $\sigma > 20$, we apply multi-pass denoising scheme with 6 iterations, *i.e.*, the output of the previous pass is weighted averaged with the original noisy image (weights of 0.9 and 0.1 for the previous output and the noisy image, respectively).

We compare the proposed Online Self-MM with various popular or state-of-the-art denoising algorithms, including (1) classic non-local methods BM3D [5] and C-BM3D [4], (2) state-of-the-art deep denoisers FFDNet [40] and FOCNet [14], and (3) guided denoising methods Guided Filtering [11] and Cross-Field Filtering [37]. To denoise four-channel data, for classic algorithms, we apply channel-wise BM3D denoising, and BM3D + C-BM3D to denoise NIR and RGB, respectively; for deep denoisers, we apply the RGB and gray version of FFDNet to denoise RGB and NIR components, and FOCNet to channel-wise denoising. Besides, as the guided denoising methods [11, 37] are for general image fusion (*i.e.*, not mainly for denoising), and require the guidance channel to be clean, we follow the same setups with the oracle clean NIR channels available as guidance. To compare, we vary the proposed Online Self-MM to denoising only RGB channels, denoted as “Only RGB”. Furthermore, to better understand the proposed Online Self-MM scheme, we perform ablation study, by running our algorithm but only (i) applying low-rank penalties (denoted as “w/o TL”) and (ii)

⁴We tested 20 images of the same size and record the average runtime, while variance is very small.

⁵We applied other settings, *e.g.*, using a larger stride, and obtained similar or proportional speedups.

applying transform learning regularizer (denoted as “w/o LR”). Table 3 lists the PSNRs (in dB) of RGB-NIR denoising results for different noise levels, which are averaged over the randomly selected 18 images from the IVRG RGB-NIR Dataset [1]. The proposed algorithm outperforms all competing methods in average, and for most noise levels. Besides, as a self-supervised learning algorithm, our method generates superior results when σ is low. On the contrary, deep algorithms demonstrate advantages when the data become more noisy. Fig. 3 shows examples of the denoised RGB-NIR images ($\sigma = 50$), in which our method preserves more detailed textures and alleviates distortion with better visual quality, compared to competing methods.

6 Conclusion

We proposed a novel Self-Convolution operator to unify non-local image modeling. We showed that Self-Convolution generalizes many commonly used non-local schemes, including block matching and non-local means. Based on Self-Convolution, we also proposed a multi-modality image restoration scheme called Online Self-MM. Extensive experiments show that (1) Self-Convolution can speed up block matching up to $9\times$ in many popular algorithms and (2) Self-MM outperforms state-of-the-art algorithms for denoising RGB-NIR images. We plan to jointly optimize Self-Convolution and non-local algorithms in future work.

7 Appendix

7.1 Proofs for Unified Non-Local Modeling via Self-Convolution

We present the detailed proofs regarding the proposed Self-Convolution formulation (5), where the Self-Convolution \mathbf{C}_i is computed as (4).

First of all, we prove Lemma 1 which shows the connection between (4) and the normalized cross correlation [29]. The latter for the case of (non-negative) natural images leads to

$$d_{NCC}(\mathbf{X}_j, \mathbf{X}_i) = -\frac{\text{vec}(\mathbf{X}_j)^T \text{vec}(\mathbf{X}_i)}{\|\mathbf{X}_j\|_F \|\mathbf{X}_i\|_F}, \quad (15)$$

where $\mathbf{h}_{X_i} = \|\mathbf{X}_i\|_F \mathbf{h}_X$ denotes a normalization vector for each \mathbf{X}_i , and $\mathbf{h}_X(j) \triangleq \|\mathbf{X}_j\|_F$.

Lemma 1. *The normalized cross-correlation in (15) is $d_{NCC}(\mathbf{X}_j, \mathbf{X}_i) = -[\text{vec}(\mathbf{C}_i) \odot \mathbf{g}_{X_i}](j)$, where $\mathbf{g}_{X_i}(j) = 1/\mathbf{h}_{X_i}(j) \forall j$.*

Proof of Lemma 1. By converting the 2D coordinates (j, k) used in (4) into 1D as (j) , and vectorizing the reference patch \mathbf{X}_i and the Self-Convolution matrix \mathbf{C}_i , (4) is equivalent to

$$\text{vec}(\mathbf{C}_i)(j) = \sum_{l=1}^n \text{vec}(\mathbf{X}_i)(l) \times \text{vec}(\mathbf{X}_j)(l) = \text{vec}(\mathbf{X}_i)^T \text{vec}(\mathbf{X}_j). \quad (16)$$

where \mathbf{X}_j denotes the j -th patch (with its top left corner at pixel (j,k) as in (4)) that is extracted from \mathbf{X} . Therefore, the normalized cross-correlation defined by (15) is

$$d_{NCC}(\mathbf{X}_j, \mathbf{X}_i) = -\frac{\text{vec}(\mathbf{X}_j)^T \text{vec}(\mathbf{X}_i)}{\|\mathbf{X}_j\|_F \|\mathbf{X}_i\|_F} = -\frac{\text{vec}(\mathbf{C}_i)(j)}{\mathbf{h}_{X_i}(j)} = -[\text{vec}(\mathbf{C}_i) \odot \mathbf{g}_{X_i}](j), \quad (17)$$

where $\mathbf{g}_{X_i}(j) = 1/\mathbf{h}_{X_i}(j) \forall j$. \square

Next, we prove the Lemma 2 which shows the connection between (4) and the Euclidean distance defined as

$$d_E(\mathbf{X}_j, \mathbf{X}_i) = \|\mathbf{X}_j - \mathbf{X}_i\|_F^2. \quad (18)$$

Lemma 2. *The Euclidean distance in (18) is $d_E(\mathbf{X}_j, \mathbf{X}_i) = [\mathbf{h}_X \odot \mathbf{h}_X + \|\mathbf{X}_i\|_F^2 \mathbf{1} - 2\text{vec}(\mathbf{C}_i)](j) \forall j$.*

Proof of Lemma 2. The Euclidean distance defined by (18) is

$$d_E(\mathbf{X}_j, \mathbf{X}_i) = \|\mathbf{X}_j - \mathbf{X}_i\|_F^2 = \|\mathbf{X}_j\|_F^2 + \|\mathbf{X}_i\|_F^2 - 2\text{vec}(\mathbf{X}_i)^T \text{vec}(\mathbf{X}_j). \quad (19)$$

Here, $\|\mathbf{X}_j\|_F^2 = [\mathbf{h}_X \odot \mathbf{h}_X](j)$. Besides, according to (16) from the proof for Lemma 1, we have $2\text{vec}(\mathbf{X}_i)^T \text{vec}(\mathbf{X}_j) = 2\text{vec}(\mathbf{C}_i)(j)$. Therefore, the Euclidean distance is

$$\begin{aligned} d_E(\mathbf{X}_j, \mathbf{X}_i) &= [\mathbf{h}_X \odot \mathbf{h}_X](j) + \|\mathbf{X}_i\|_F^2 - 2\text{vec}(\mathbf{C}_i)(j) \\ &= [\mathbf{h}_X \odot \mathbf{h}_X + \|\mathbf{X}_i\|_F^2 \mathbf{1} - 2\text{vec}(\mathbf{C}_i)](j). \end{aligned} \quad (20)$$

\square

We now prove Proposition 1 which shows the equivalence between the Self-Convolution Formulation (5) and the non-local means (NLM) algorithm, which computes the weighting coefficients with respect to other patches as follows:

$$\mathbf{s}_i(j) = \Theta_i^{-1} \exp(-\|\mathbf{X}_j - \mathbf{X}_i\|_F^2 / b^2), \quad \Theta_i = \sum_j \exp(-\|\mathbf{X}_j - \mathbf{X}_i\|_F^2 / b^2) \quad \forall i, \quad (21)$$

where b is a hyper-parameter scaling the distance metric.

Proposition 1. *Self-Convolution formulation in (5) is equivalent to the weight calculation in NLM (21) if $\rho(\mathbf{a}_i) = 0$ and $H(\mathbf{C}_i, \mathbf{X}, \mathbf{X}_i) = \frac{1}{\Theta_i} \exp\{(2\text{vec}(\mathbf{C}_i) - \mathbf{h}_X \odot \mathbf{h}_X - \|\mathbf{X}_i\|_F^2 \mathbf{1})/b^2\}$. Thus, the result of (5) becomes the NLM weighting, i.e., $\hat{\mathbf{a}}_i = \hat{\mathbf{s}}_i$ coincides with (21).*

Proof of Proposition 1. The Euclidean distance in the exponent in (21) can be rewritten using Lemma 2. Then, with $\rho(\mathbf{a}_i) = 0$ and $H(\mathbf{C}_i, \mathbf{X}, \mathbf{X}_i) = \frac{1}{\Theta_i} \exp\{(2\text{vec}(\mathbf{C}_i) - \mathbf{h}_X \odot \mathbf{h}_X - \|\mathbf{X}_i\|_F^2 \mathbf{1})/b^2\}$ ($\exp\{\cdot\}$ denotes vector-wise exponential function), the Self-Convolution formulation (5) reduces to the following form

$$\hat{\mathbf{a}}_i = \arg \min_{\mathbf{a}_i} \left\| \frac{1}{\Theta_i} \exp\{(2\text{vec}(\mathbf{C}_i) - \mathbf{h}_X \odot \mathbf{h}_X - \|\mathbf{X}_i\|_F^2 \mathbf{1})/b^2\} - \mathbf{a}_i \right\|_F^2 \quad \forall i, \quad (22)$$

which has an exact least-squares solution as $\hat{\mathbf{a}}_i = \frac{1}{\Theta_i} \exp\{(2\text{vec}(\mathbf{C}_i) - \mathbf{h}_X \odot \mathbf{h}_X - \|\mathbf{X}_i\|_F^2 \mathbf{1})/b^2\}$. Based on Lemma 2, $\hat{\mathbf{a}}_i(j) = \frac{1}{\Theta_i} \exp(-\|\mathbf{X}_j - \mathbf{X}_i\|_F^2/b^2)$ which completes the proof. \square

Finally, we prove the Theorem 1 which shows the equivalence between the Self-Convolution Formulation (5) and the block matching (BM) algorithm. The BM algorithm using Euclidean distance metric is defined as (2). Besides, the BM algorithm using the normalized cross correlation as the metric is defined as (3).

Theorem 1. *Self-Convolution formulation is equivalent to block matching when*

1. $\rho(\mathbf{a}_i) = \Phi_K(\mathbf{a}_i)$, where $\Phi_K(\mathbf{a}_i) = 0$ if $\|\mathbf{a}_i\|_0 \leq K$ and $\Phi_K(\mathbf{a}_i) = +\infty$ otherwise.
2. $H(\mathbf{C}_i, \mathbf{X}, \mathbf{X}_i) = \text{vec}(\mathbf{C}_i) - \frac{1}{2} \mathbf{h}_X \odot \mathbf{h}_X$ using Euclidean distance; Or
3. $H(\mathbf{C}_i, \mathbf{X}, \mathbf{X}_i) = \text{vec}(\mathbf{C}_i) \odot \mathbf{g}_{X_i}$ using normalized cross correlation.

Thus, the support of the solution to (5), i.e., $\text{supp}(\hat{\mathbf{a}}_i)$ is the solution \hat{S}_i^E in (2) or \hat{S}_i^{NCC} in (3).

Proof of Theorem 1. First, when $\rho(\mathbf{a}_i) = \Phi_K(\mathbf{a}_i)$ and $H(\mathbf{C}_i, \mathbf{X}, \mathbf{X}_i) = \text{vec}(\mathbf{C}_i) - \frac{1}{2} \mathbf{h}_X \odot \mathbf{h}_X$, the Self-Convolution formulation is reduced to

$$\hat{\mathbf{a}}_i = \arg \min_{\mathbf{a}_i} \left\| \text{vec}(\mathbf{C}_i) - \frac{1}{2} \mathbf{h}_X \odot \mathbf{h}_X - \mathbf{a}_i \right\|_F^2 + \Phi_K(\mathbf{a}_i) \quad \forall i. \quad (23)$$

As the penalty term $\Phi_K(\mathbf{a}_i)$ is a barrier function, which is equivalent to imposing an ℓ_0 sparsity constraint. Therefore, the equivalent constrained optimization problem is

$$\hat{\mathbf{a}}_i = \arg \min_{\mathbf{a}_i} \left\| \text{vec}(\mathbf{C}_i) - \frac{1}{2} \mathbf{h}_X \odot \mathbf{h}_X - \mathbf{a}_i \right\|_F^2 \quad \text{s.t.} \quad \|\mathbf{a}_i\|_0 \leq K \quad \forall i. \quad (24)$$

Denote $\mathbf{b}_i \triangleq \text{vec}(\mathbf{C}_i) - \frac{1}{2} \mathbf{h}_X \odot \mathbf{h}_X$. The exact solution to (24) is obtained by projecting \mathbf{b}_i onto the ℓ_0 ball. Thus the optimal $\hat{\mathbf{a}}_i$ can be computed as

$$\hat{\mathbf{a}}_i(j) = \begin{cases} \mathbf{b}_i(j) & , j \in \Omega_K^i \\ 0 & , j \notin \Omega_K^i \end{cases} \quad (25)$$

Here the set $\Omega_K^i = \text{supp}(\hat{\mathbf{a}}_i)$ indexes the top-K elements of largest magnitude in \mathbf{b}_i , which are identical to the solution to (26) below.

$$\Omega_K^i = \arg \max_{\mathcal{S}_i: |\mathcal{S}_i| \leq K} \sum_{j \in \mathcal{S}_i} \mathbf{b}_i(j) \quad (26)$$

Furthermore, based on Lemma 2, we have

$$\mathbf{b}_i = \text{vec}(\mathbf{C}_i) - \frac{1}{2} \mathbf{h}_X \odot \mathbf{h}_X = -d_E(\mathbf{X}_j, \mathbf{X}_i) + \frac{1}{2} \|\mathbf{X}_i\|_F^2 \mathbf{1}. \quad (27)$$

Substituting (27) to (26), we prove the equivalence using **Euclidean distance** as

$$\text{supp}(\hat{\mathbf{a}}_i) = \arg \max_{\mathcal{S}_i: |\mathcal{S}_i| \leq K} \sum_{j \in \mathcal{S}_i} \left\{ -d_E(\mathbf{X}_j, \mathbf{X}_i) + \frac{1}{2} \|\mathbf{X}_i\|_F^2 \mathbf{1} \right\} = \arg \min_{\mathcal{S}_i: |\mathcal{S}_i| \leq K} \sum_{j \in \mathcal{S}_i} d_E(\mathbf{X}_j, \mathbf{X}_i). \quad (28)$$

Next, when $\rho(\mathbf{a}_i) = \Phi_K(\mathbf{a}_i)$ and $H(\mathbf{C}_i, \mathbf{X}, \mathbf{X}_i) = \text{vec}(\mathbf{C}_i) \odot \mathbf{g}_{X_i}$, the Self-Convolution formulation (5) reduces to the following form

$$\hat{\mathbf{a}}_i = \arg \min_{\mathbf{a}_i} \left\| \text{vec}(\mathbf{C}_i) \odot \mathbf{g}_{X_i} - \mathbf{a}_i \right\|_F^2 \quad \text{s.t.} \quad \|\mathbf{a}_i\|_0 \leq K \quad \forall i. \quad (29)$$

Method	Classic		Deep	Guided		Online Self-MM			
	BM3D [5]	C-BM3D [4]	FOCNet [14]	Guided Filter [11]	Cross Field [37]	Only Left	w/o TL	w/o LR	Proposed
5	37.28	38.34	-	24.96	34.83	38.65	38.51	38.12	38.65
10	32.92	34.17	-	24.76	30.06	34.43	34.29	33.97	34.49
15	30.59	31.90	-	24.45	27.69	32.07	32.01	31.76	32.17
20	29.03	30.36	-	24.07	25.94	30.39	30.42	30.06	30.64
50	24.39	25.79	25.65	23.97	21.06	25.89	25.78	25.42	25.91

Table 4: PSNRs (in dB) of the Stereo image denoising results, averaged over 24 images selected from the Flickr1024 Stereo Dataset [28, 26]. For those noise levels for which FOCNet’s trained models are not publicly available, we put “-” as the corresponding results are unavailable.

Similarly as in (25), there is an exact solution to (29) by setting $\mathbf{b}_i \triangleq \text{vec}(\mathbf{C}_i) \odot \mathbf{g}_{X_i}$ in (25). Based on Lemma 1 and (26), we prove the equivalence using **normalized cross correlation** as

$$\text{supp}(\hat{\mathbf{a}}_i) = \arg \max_{S_i: |S_i| \leq K} \sum_{j \in S_i} [\text{vec}(\mathbf{C}_i) \odot \mathbf{g}_{X_i}](j) = \arg \min_{S_i: |S_i| \leq K} \sum_{j \in S_i} -[\text{vec}(\mathbf{C}_i) \odot \mathbf{g}_{X_i}](j). \quad (30)$$

□

7.2 Additional Experiments

Dataset: The IVRG RGB-NIR Dataset [1] has been explained in the main paper. Flickr1024 Stereo Dataset [28, 26] contains 1024 high-quality image pairs of left and right images, categorized into diverse scenarios. We randomly select 2 pairs from 12 different scenarios mentioned in [28], including animals, building, indoors, landscapes, macroshots, nights, people, plants, sculptures, streets, synthetics, and vehicles, *i.e.*, 24 pairs in all, as testing images. The selected testing images contain 6 channels, with spatial resolutions around 800×1000 . We simulate i.i.d. additive Gaussian noise for all 6 channels with different $\sigma = 5, 10, 15, 20$, and 50 for each image.

Implementation Details and Parameters: The proposed Multi-Modality image denoising scheme uses a self-supervised approach, and there are several hyperparameters used in the algorithm, among which we directly use the noisy image as the initial estimate $\hat{\mathbf{Y}}_0$. We work with 3D patches of size $6 \times 6 \times 3$ for the Stereo dataset, and set the spatial search window as $\sqrt{N} \times \sqrt{N} \times C = 30 \times 30 \times 6$. We initialize the unitary sparsifying transform \mathbf{W}_0 to be the 3D DCT. The sparsity and low-rank penalty weights γ_s and γ_l are set to 1. As for 3D searching (Stereo Dataset), we apply the multi-pass denoising scheme at each noise level. For low-noise cases (*i.e.*, $0 \leq \sigma \leq 20$), we set the number of passes to 4, while for high-noise cases (*i.e.*, $\sigma > 20$), we set the number of passes to 6. For every pass, the input image $\hat{\mathbf{Y}}_t$ is a linear combination of the denoised estimate $\hat{\mathbf{Y}}_{t-1}$ from the last pass and the original noisy image $\tilde{\mathbf{Y}}$, where we set the weight for the noisy image to $\delta = 0.1$. Then, we re-estimate the variance of $\hat{\mathbf{Y}}_t$ based on $\sigma_t^2 = \psi^2(\sigma^2 - (1/N) \|\tilde{\mathbf{Y}} - \hat{\mathbf{Y}}_t\|_2^2)$, where the factor ψ is set to be 0.56 to alleviate the over-estimated noise level [10, 23]. For low noise level cases, at passes $t = 1, 2, \dots, 4$, we set the penalty parameter in (10) $\beta = [3.0, 2.4, 2.0, 0.8]$ and $\theta = 1.2\sigma_{t-1}$; for high noise level cases, at passes $t = 1, 2, \dots, 6$, we set the penalty parameter $\beta = [3.0, 2.4, 2.0, 1.2, 1, 0.8]$ and $\theta = 1.0\sigma_{t-1}$. Additionally, we set the number of matched similar patches to $K = 20$, for $\sigma = 5, 10, 15, 20$, and $K = 25$ for $\sigma=50$, respectively.

Comparisons with State-of-the-Art Methods: We compare the proposed Online Self-MM with various popular or state-of-the-art denoising algorithms for the Stereo dataset (24 images), including (1) classic non-local methods BM3D [5] and C-BM3D [4], (2) state-of-the-art deep denoiser FOCNet [14], and (3) guided denoising methods Guided Filtering [11] and Cross-Field Filtering [37]. To denoise the six-channel data, for classic algorithms, we apply channel-wise BM3D denoising, or the C-BM3D twice to denoise left and right images, respectively; for deep denoisers, we apply FOCNet for channel-wise denoising. Besides, as the guided denoising methods [11, 37] are for general image fusion (*i.e.*, not mainly for denoising), and require the guidance channel to be clean, we follow the same setups with the clean (oracle) right view channels available as guidance. To compare, we modify the proposed Online Self-MM scheme to denoise only left image channels, denoted as “Only Left”. Furthermore, to better understand the proposed Online Self-MM scheme, we perform an ablation study, by running our algorithm but only (i) applying low-rank penalties (denoted as “w/o TL”), or only (ii) applying the transform learning regularizer (denoted as “w/o LR”). Table 4 lists the PSNRs (in dB) of Stereo image denoising results for different noise levels, which are averaged



(a) Ground truth

(b) Noisy

(c) C-BM3D

(d) Ours

Figure 4: Examples of the Stereo image denoising ($\sigma = 50$) results (the first row is left image and the second row is right image): (a) ground truth, (b) noisy Stereo image input, (c) the denoised Stereo image using C-BM3D, and (d) the proposed Online Self-MM results.

over the randomly selected 24 images from the Stereo dataset. The proposed algorithm outperforms all competing methods on average, and for all noise levels. Fig. 4 shows examples of the denoised Stereo images ($\sigma = 50$), where the proposed method preserves more detailed textures and alleviates distortion with better visual quality, compared to competing methods.

References

- [1] Brown, M., Süssstrunk, S.: Multispectral SIFT for scene category recognition. In: Computer Vision and Pattern Recognition (CVPR11). pp. 177–184. Colorado Springs (June 2011)
- [2] Buades, A., Coll, B., Morel, J.M.: A non-local algorithm for image denoising. In: 2005 IEEE Computer Society Conference on Computer Vision and Pattern Recognition (CVPR'05). vol. 2, pp. 60–65. IEEE (2005)
- [3] Cooley, J.W., Tukey, J.W.: An algorithm for the machine calculation of complex fourier series. *Mathematics of computation* **19**(90), 297–301 (1965)
- [4] Dabov, K., Foi, A., Katkovnik, V., Egiazarian, K.: Color image denoising via sparse 3D collaborative filtering with grouping constraint in luminance-chrominance space. In: 2007 IEEE International Conference on Image Processing. vol. 1, pp. I–313. IEEE (2007)
- [5] Dabov, K., Foi, A., Katkovnik, V., Egiazarian, K.: Image denoising by sparse 3-D transform-domain collaborative filtering. *IEEE Transactions on image processing* **16**(8), 2080–2095 (2007)
- [6] Dong, W., Li, G., Shi, G., Li, X., Ma, Y.: Low-rank tensor approximation with laplacian scale mixture modeling for multiframe image denoising. In: Proceedings of the IEEE International Conference on Computer Vision. pp. 442–449 (2015)
- [7] Dong, W., Shi, G., Li, X.: Nonlocal image restoration with bilateral variance estimation: a low-rank approach. *IEEE transactions on image processing* **22**(2), 700–711 (2012)
- [8] Dong, W., Zhang, L., Shi, G., Li, X.: Nonlocally centralized sparse representation for image restoration. *IEEE transactions on Image Processing* **22**(4), 1620–1630 (2012)
- [9] Elad, M., Aharon, M.: Image denoising via sparse and redundant representations over learned dictionaries. *IEEE Transactions on Image processing* **15**(12), 3736–3745 (2006)
- [10] Gu, S., Zhang, L., Zuo, W., Feng, X.: Weighted nuclear norm minimization with application to image denoising. In: Proceedings of the IEEE conference on computer vision and pattern recognition. pp. 2862–2869 (2014)
- [11] He, K., Sun, J., Tang, X.: Guided image filtering. *IEEE transactions on pattern analysis and machine intelligence* **35**(6), 1397–1409 (2012)
- [12] He, W., Yao, Q., Li, C., Yokoya, N., Zhao, Q.: Non-local meets global: An integrated paradigm for hyperspectral denoising. In: 2019 IEEE/CVF Conference on Computer Vision and Pattern Recognition (CVPR). pp. 6861–6870. IEEE (2019)
- [13] Indyk, P., Kapralov, M.: Sample-optimal fourier sampling in any constant dimension. In: 2014 IEEE 55th Annual Symposium on Foundations of Computer Science. pp. 514–523. IEEE (2014)
- [14] Jia, X., Liu, S., Feng, X., Zhang, L.: Focnet: A fractional optimal control network for image denoising. In: IEEE Conference on Computer Vision and Pattern Recognition (2019)
- [15] Katznelson, Y.: An introduction to harmonic analysis. Cambridge University Press (2004)
- [16] Liu, D., Wen, B., Fan, Y., Loy, C.C., Huang, T.S.: Non-local recurrent network for image restoration. In: Advances in Neural Information Processing Systems. pp. 1673–1682 (2018)
- [17] Maggioni, M., Boracchi, G., Foi, A., Egiazarian, K.: Video denoising, deblocking, and enhancement through separable 4-d nonlocal spatiotemporal transforms. *IEEE Transactions on image processing* **21**(9), 3952–3966 (2012)
- [18] Mairal, J., Bach, F., Ponce, J., Sapiro, G., Zisserman, A.: Non-local sparse models for image restoration. In: 2009 IEEE 12th international conference on computer vision. pp. 2272–2279. IEEE (2009)
- [19] Mathieu, M., Henaff, M., LeCun, Y.: Fast training of convolutional networks through FFTs. arXiv preprint arXiv:1312.5851 (2013)
- [20] Parmar, N., Vaswani, A., Uszkoreit, J., Kaiser, Ł., Shazeer, N., Ku, A., Tran, D.: Image transformer. arXiv preprint arXiv:1802.05751 (2018)
- [21] Ravishanker, S., Bresler, Y.: Learning sparsifying transforms. *IEEE Transactions on Signal Processing* **61**(5), 1072–1086 (2012)

- [22] Ravishankar, S., Bresler, Y.: Closed-form solutions within sparsifying transform learning. In: 2013 IEEE international conference on acoustics, speech and signal processing. pp. 5378–5382. IEEE (2013)
- [23] Romano, Y., Elad, M.: Boosting of image denoising algorithms. *SIAM Journal on Imaging Sciences* **8**(2), 1187–1219 (2015)
- [24] Vasilache, N., Johnson, J., Mathieu, M., Chintala, S., Piantino, S., LeCun, Y.: Fast convolutional nets with fbfft: A gpu performance evaluation. arXiv preprint arXiv:1412.7580 (2014)
- [25] Vaswani, A., Shazeer, N., Parmar, N., Uszkoreit, J., Jones, L., Gomez, A.N., Kaiser, Ł., Polosukhin, I.: Attention is all you need. In: *Advances in neural information processing systems*. pp. 5998–6008 (2017)
- [26] Wang, L., Wang, Y., Liang, Z., Lin, Z., Yang, J., An, W., Guo, Y.: Learning parallax attention for stereo image super-resolution. In: *Proceedings of the IEEE Conference on Computer Vision and Pattern Recognition*. p. 12250–12259 (2019)
- [27] Wang, X., Girshick, R., Gupta, A., He, K.: Non-local neural networks. In: *Proceedings of the IEEE conference on computer vision and pattern recognition*. pp. 7794–7803 (2018)
- [28] Wang, Y., Wang, L., Yang, J., An, W., Guo, Y.: Flickr1024: A large-scale dataset for stereo image super-resolution. In: *The IEEE International Conference on Computer Vision (ICCV) Workshops*. pp. 3852–3857 (Oct 2019)
- [29] Wei, S.D., Lai, S.H.: Fast template matching based on normalized cross correlation with adaptive multilevel winner update. *IEEE Transactions on Image Processing* **17**(11), 2227–2235 (2008)
- [30] Wen, B., Ravishankar, S., Bresler, Y.: Structured overcomplete sparsifying transform learning with convergence guarantees and applications. *Int. Journal of Computer Vision (IJCV)* **114**(2), 137–167 (2015)
- [31] Wen, B., Li, Y., Bresler, Y.: When sparsity meets low-rankness: Transform learning with non-local low-rank constraint for image restoration. In: *IEEE International Conference on Acoustics, Speech and Signal Processing (ICASSP)*. pp. 2297–2301. IEEE (2017)
- [32] Wen, B., Li, Y., Bresler, Y.: Image recovery via transform learning and low-rank modeling: The power of complementary regularizers. *IEEE Transactions on Image Processing* **29**, 5310–5323 (2020)
- [33] Wen, B., Li, Y., Pfister, L., Bresler, Y.: Joint adaptive sparsity and low-rankness on the fly: an online tensor reconstruction scheme for video denoising. In: *Proceedings of the IEEE International Conference on Computer Vision*. pp. 241–250 (2017)
- [34] Xu, J., Zhang, L., Zhang, D.: A trilateral weighted sparse coding scheme for real-world image denoising. In: *Proceedings of the European Conference on Computer Vision (ECCV)*. pp. 20–36 (2018)
- [35] Xu, J., Zhang, L., Zhang, D., Feng, X.: Multi-channel weighted nuclear norm minimization for real color image denoising. In: *Proceedings of the IEEE International Conference on Computer Vision*. pp. 1096–1104 (2017)
- [36] Xu, J., Zhang, L., Zuo, W., Zhang, D., Feng, X.: Patch group based nonlocal self-similarity prior learning for image denoising. In: *Proceedings of the IEEE international conference on computer vision*. pp. 244–252 (2015)
- [37] Yan, Q., Shen, X., Xu, L., Zhuo, S., Zhang, X., Shen, L., Jia, J.: Cross-field joint image restoration via scale map. In: *Proceedings of the IEEE International Conference on Computer Vision*. pp. 1537–1544 (2013)
- [38] Zha, Z., Yuan, X., Wen, B., Zhou, J., Zhang, J., Zhu, C.: From rank estimation to rank approximation: Rank residual constraint for image restoration. *IEEE Transactions on Image Processing* (2019)
- [39] Zhang, H., Goodfellow, I., Metaxas, D., Odena, A.: Self-attention generative adversarial networks. arXiv preprint arXiv:1805.08318 (2018)
- [40] Zhang, K., Zuo, W., Zhang, L.: Ffdnet: Toward a fast and flexible solution for cnn-based image denoising. *IEEE Transactions on Image Processing* **27**(9), 4608–4622 (2018)
- [41] Zuo, W., Zhang, L., Song, C., Zhang, D.: Texture enhanced image denoising via gradient histogram preservation. In: *Proceedings of the IEEE Conference on Computer Vision and Pattern Recognition*. pp. 1203–1210 (2013)